

Searching for the scale of homogeneity

Vicent J. Martínez,^{1*} María-Jesús Pons-Bordería,^{2†} Rana A. Moyeed^{3‡}
and Matthew J. Graham^{1,4§}

¹Departament d'Astronomia i Astrofísica, Universitat de València, E-46100 Burjassot, València, Spain

²Departamento de Física Teórica, Universidad Autónoma de Madrid, 28049 Cantoblanco, Madrid, Spain

³School of Mathematics and Statistics, University of Plymouth, Drake Circus, Plymouth PL4 8AA, U.K.

⁴Centre for Astrophysics, University of Central Lancashire, Preston PR1 2HE, U.K.

Accepted 1997 ???? ?. Received 1997 ???? ?; in original form 1996 ???? ??

ABSTRACT

We introduce a statistical quantity, known as the K function, related to the integral of the two-point correlation function. It gives us straightforward information about the scale where clustering dominates and the scale at which homogeneity is reached. We evaluate the correlation dimension, D_2 , as the local slope of the log–log plot of the K function. We apply this statistic to several stochastic point fields, to three numerical simulations describing the distribution of clusters and finally to real galaxy redshift surveys. Four different galaxy catalogues have been analysed using this technique: the Center for Astrophysics I, the Perseus–Pisces redshift surveys (these two lying in our local neighbourhood), the Stromlo–APM and the 1.2 Jy *IRAS* redshift surveys (these two encompassing a larger volume). In all cases, this cumulant quantity shows the fingerprint of the transition to homogeneity. The reliability of the estimates is clearly demonstrated by the results from controllable point sets, such as the segment Cox processes. In the cluster distribution models, as well as in the real galaxy catalogues, we never see long plateaus when plotting D_2 as a function of the scale, leaving no hope for unbounded fractal distributions.

Key words: methods: statistical; galaxies: clustering; large-scale structure of Universe

1 INTRODUCTION

The standard cosmology is based on the assumption that the Universe must be homogeneous on very large scales. Several pieces of evidence support this assumption: the homogeneity and isotropy of the microwave background radiation (Smoot et al. 1992) and some aspects of the large scale distribution of matter (Peebles 1989) seem to strongly advocate uniformity on scales bigger than about $200 h^{-1}$ Mpc (where $H_0 = 100 h \text{ km s}^{-1} \text{ Mpc}^{-1}$).

However the presence of very large features in the galaxy distribution like the Bootes void (Kirshner et al. 1981) or the Great Wall (Geller & Huchra 1989) which span a scale length of the order of $100 h^{-1}$ Mpc calls the actual scale of homogeneity into question. Moreover other authors consider the assumption of homogeneity just a theoretical

prejudice not necessarily supported by the observational evidence quoted above. They defend the alternative idea of an unbounded fractal cosmology (Coleman & Pietronero 1992). Guzzo (1997) argues against this interpretation on the basis of a careful handling of the data.

The spatial two-point correlation function is the statistical tool mainly used to describe the clustering in the Universe (Peebles 1980, 1993). However, because of the integral constraint (Peebles 1980), one cannot estimate it at very large distances from the currently available redshift surveys. In order to study clustering in the regime where it is not very strong, we have only two possibilities: either we extend the size of the redshift catalogues or we use alternative statistical descriptors. The approach described in this paper points in the latter direction. In the same line, other authors (Fisher et al 1993; Park et al. 1994; Tadros & Efstathiou 1996) have tried to measure the power-spectrum on large scales directly from galaxy catalogues. Einasto & Gramman (1993) studied the transition to homogeneity by means of the power-spectrum and found a relation between

* Email: martinez@quasar.daa.uv.es

† Email: pons@astro1.ft.uam.es

‡ Email: rmoyeed@plymouth.ac.uk

§ Email: m.j.graham@uclan.ac.uk

the correlation transition scale and the spectral transition scale (turnover in $P(k)$).

We introduce the quantity called $K(r)$, which is related to the correlation function $\xi(r)$. The novelty of our approach lies essentially in the fact that we shall use a cumulant quantity instead of a differential quantity such as $\xi(r)$. Although for a point process the functions $\xi(r)$ and $K(r)$ are well defined, what we measure from the galaxy catalogues are just estimators of those functions. One of our main claims is that the estimators for $K(r)$ are more reliable than the most currently used estimators for $\xi(r)$ and that makes its use recommendable (especially in three-dimensional processes and at large scales) despite its somewhat less informative character.

2 THE K FUNCTION AND THE CORRELATION DIMENSION

Within the field of the statistical analysis of point fields, new techniques and estimators of the clustering of spatial point patterns have been developed in the past decades. Unfortunately, the connection between this set of scholars and cosmologists is not as important today as it was in the late fifties when the Berkeley statisticians Neymann and Scott carried out an intensive programme about the analysis of the Lick catalogue (Neymann & Scott 1952, 1955). Today, one of the most popular summary statistics for point patterns is the K -function (Bartlett 1964, Ripley 1976, 1977, 1981). Let us introduce this quantity using the terminology employed by statisticians and stressing its connections with the quantities used in cosmology (see also Szapudi & Szalay 1997 for a different application of Ripley's statistic to cosmology).

Let us consider a point process acting on a region $D \subset \mathbf{R}^3$ with volume V whose output is a collection of positions of N galaxies (or clusters of galaxies) $\{\mathbf{x}_i\}$. If we take two infinitesimal volumes dV_1 and dV_2 around \mathbf{x}_1 and \mathbf{x}_2 respectively, the joint probability of there being a point lying in each of these volumes reads:

$$dP = \lambda_2(\mathbf{x}_1, \mathbf{x}_2) dV_1 dV_2, \quad (1)$$

where λ_2 is the so-called second order intensity function (Diggle 1983). If the process is stationary (invariant under translation) and isotropic (invariant under rotation), then $\lambda_2(\mathbf{x}_1, \mathbf{x}_2) = \lambda_2(|\mathbf{x}_1 - \mathbf{x}_2|)$. The two-point correlation function can be expressed by means of it as:

$$\xi(r) = \frac{\lambda_2(r)}{n^2} - 1 \quad (2)$$

where $r = |\mathbf{x}_1 - \mathbf{x}_2|$ and n is the mean number density in a fair sample.

The second-order cumulative function $K(r)$ is defined so that the expected number of neighbours a given galaxy will have at a distance less than r is $nK(r)$. Therefore its relation with the two-point correlation function is

$$K(r) = \int_0^r 4\pi s^2 (1 + \xi(s)) ds \quad (3)$$

For a homogeneous Poisson process this function is just

$$K_{\text{Pois}}(r) = \frac{4\pi}{3} r^3. \quad (4)$$

2.1 Relation with other cumulant quantities

Other second-order cumulant functions have been used in the statistical analysis of the large scale structure in the Universe. Within the context of the scaling or multifractal approach the partition function $Z(q, r)$ introduced in the description of the galaxy clustering by Martínez et al. (1990) is formally related with $K(r)$ for the second moment ($q = 2$) by $Z(2, r) = K(r)/V$ where V is the volume of the sample. Borgani et al. (1994) perform an exhaustive analysis of the cluster distribution in both real catalogues of clusters of galaxies and simulations by means of the $Z(q, r)$ function. In that paper the authors give an expression for using this partition function when a selection function has to be considered. The dependence of the results of $Z(q, r)$ of the particular volume of the sample has led some authors (Domínguez-Tenreiro, Gómez-Flechoso and Martínez 1994) to normalize $Z(2, r)$ in order to get a function Z_{norm} which coincides for different samples (within different volumes) in the homogeneous regime. Basically this normalization makes Z_{norm} equivalent to $K(r)$.

Peebles (1980) introduced the moments of the counts of neighbours $\langle N \rangle_r$ as the mean count of objects in balls of radius r excluding the central one. By definition $\langle N \rangle_r$ is the correlation integral $C(r)$ used by Martínez et al. (1995) in the analysis of the multiscaling properties of the matter distribution and is related with $K(r)$ simply by $\langle N \rangle_r = nK(r) = C(r)$. In fact, other authors (Martínez & Coles 1994; McCauley 1997) have chosen the normalization for the partition function $Z(q, r)$ in such a way that $\langle N \rangle_r = Z(2, r)$ directly.

Taking the shape of the K function for a random object distribution (Poisson process) into account, one can just consider the difference between $K(r)$ and $K_{\text{Pois}}(r)$ which leads to another cumulant quantity commonly used in the statistical description of the galaxy clustering, $4\pi J_3(r) = K(r) - K_{\text{Pois}}(r)$, where (Peebles 1980, 1993)

$$J_3(r) = \int_0^r \xi(s) s^2 ds. \quad (5)$$

Finally, if one considers the quotient instead of the difference, one gets the integral quantity used by Coleman & Pietronero (1992):

$$\Gamma^*(r) = \frac{nK(r)}{K_{\text{Pois}}(r)}, \quad (6)$$

(see also Cappi et al. (1998) for a discussion on the methods used by Pietronero and collaborators).

The advantages of the use of $K(r)$ with respect to other cumulant quantities are the following:

(i) $K(r)$ is well normalized. We can compare directly the K function of different samples, with different number density and within different volumes without extra normalization.

(ii) $K(r)$ is a well-known quantity in the field of spatial statistics and several analytical results regarding its shape and variance are already available for a variety of point processes.

(iii) It is very important to estimate the quantity $K(r)$ directly from the data and not through numerical integration of $1 + \xi(r)$, which introduces artificial smoothing of the results. Several edge-corrected unbiased estimators are avail-

able for $K(r)$. In the context of the present application, the most appreciable properties an estimator must hold are to have little variance and not to introduce spurious homogeneity by means of the edge-correction. In the next subsection we comment on different estimators for $K(r)$.

2.2 Estimators

We shall make the assumption that the process under consideration is stationary and isotropic. Such a process is also referred to as ‘statistically homogeneous’ (Peebles 1993). Note, however, that when in this paper we talk about ‘the scale of homogeneity’, we mean the scale at which the spatial distribution of the objects is uniform or indistinguishable from a homogeneous Poisson process. Nevertheless, some cluster processes are still stationary and isotropic.

There exist several estimators for K . A comparison of some of them can be found in Doguwa & Upton (1989). From the definition of K and ignoring the edge effects one could consider the following naive estimator

$$\hat{K}_N(r) = \frac{V}{N^2} \sum_{i=1}^N \sum_{\substack{j=1 \\ j \neq i}}^N \theta(r - |\mathbf{x}_i - \mathbf{x}_j|), \quad (7)$$

where θ is Heaviside’s step function, whose value is 1 when the argument is positive and 0 otherwise. Obviously for a finite sample this estimator will provide values for K smaller than the true values since neighbours outside the boundaries are not considered. One possible solution is to consider only points in an inner region as centres of the balls for counting neighbours. The points lying in the outer region, a buffer zone (Upton & Fingleton 1987; Buchert & Martínez 1993), take part in the estimator just as points which could be seen as neighbours at a given distance r of the points in the inner region. The inner region might shrink as r increases. However, this solution leads to biases (the sample is not uniformly selected), wastes a lot of data, and obviously increases the variance of the estimator (Doguwa & Upton 1989). The standard solution adopted in the statistical studies of the large-scale structures is to account for the unseen neighbours outside the sample window by means of the following edge-corrected estimator

$$\hat{K}_{DU}(r) = \frac{V}{N^2} \sum_{i=1}^N \sum_{\substack{j=1 \\ j \neq i}}^N \frac{\theta(r - |\mathbf{x}_i - \mathbf{x}_j|)}{f_i(r)}, \quad (8)$$

where $f_i(r)$ is the fraction of the volume of the sphere of radius r centred on the object i which falls within the boundaries of the sample. This kind of edge-correction has been used by Borgani et al. (1994) when calculating the partition function $Z(q, r)$ used in the multifractal analysis. In the field of spatial statistics it had been introduced by Doguwa and Upton (1989). Although this estimator has good properties, it could be slightly biased (Stoyan & Stoyan 1994). The most commonly used unbiased edge-corrected estimator in the analysis of point processes is Ripley’s estimator, which under our hypotheses reads (Baddeley et al. 1993):

$$\hat{K}_R(r) = \frac{V}{N^2} \sum_{i=1}^N \sum_{\substack{j=1 \\ j \neq i}}^N \frac{\theta(r - |\mathbf{x}_i - \mathbf{x}_j|)}{\omega_{ij}}, \quad (9)$$

Figure 1. An illustration of the weights used in the estimator of K (equation 9) in 2 dimensions. The rectangle represents the boundary of the sample. In this case, w_{ij} is the proportion of the circumference of the circle centered at \mathbf{x}_i , passing through \mathbf{x}_j , lying within the boundary of the sample. Depending on the relative positions of the galaxies with respect to the boundary, different cases are illustrated: (a) $w_{ij} = w_{ji} = 1$; (b) $w_{ij} = 1, w_{ji} < 1$; (c) $w_{ij} < 1, w_{ji} < 1$. It is clear from the plot that we weight the observed neighbour \mathbf{x}_j of the galaxy \mathbf{x}_i lying at a distance r (the radius of the circle) from it by the inverse of the probability that such a neighbour would be observed.

where the weight ω_{ij} is an edge correction equal to the proportion of the area of the sphere centred at \mathbf{x}_i and passing through \mathbf{x}_j that is contained in D ; in other words, ω_{ij} is the conditional probability that the j th point is observed given that it is at a distance r from the i th point. This correction is suitable for stationary and isotropic processes and is illustrated in Fig. 1. The unweighted K function will be negatively biased because we do not observe events outside the sampling window, so the observed counts from events which are less than a distance r from the boundary will be artificially low.

It is still possible that the best estimator depends of the kind of point process to be studied (clustered or regular) and even on the particular scale range, (see Stoyan & Stoyan (1998) for a discussion on improved estimators). We have chosen the estimator $\hat{K}_R(r)$ because of its well known good performance in a variety of cases.

In Baddeley et al. (1993) an analytic expression for ω_{ij} is given in the case D is a cube. In order to ensure that the border correction is as free of error as possible, we have chosen to generate the synthetic samples we want to analyse in a region shaped in this way. Note however that we introduce a certain bias when we estimate n through N/V but we are, on the other hand, making full use of all sample points. For all the mentioned estimators it is possible to build the corresponding versions for flux-limited samples by simply adding a weighting factor representing the selection function.

2.3 The correlation dimension

If scaling of the first moment of the count of neighbours holds, then $C(r)$ is proportional to r^{D_2} and $K(r)$ as well, since n is constant when looking at the whole region. The exponent D_2 is known as the correlation dimension and it tends to 3 on the scale r at which homogeneity is reached, hence its importance.

Once we compute K , we obtain the local dimension D_2 as the slope of a five-point log-log linear regression on the function $K(r)$ (as in Borgani et al. 1994). This local correlation dimension can be considered as a *sliding window* estimate (through the scale) of the fractal dimension (Dubuc et al. 1989). Any long plateau for a significant range of scales will be the fingerprint of a fractal range. The tendency to homogeneity will be described by an increasing behaviour of the local dimension D_2 as a function of the scale, towards the value consistent with homogeneity $D_2 = 3$. This test is much stronger than just to fit a straight line to a log-log

Figure 2. One of the realizations of each of the stochastic point processes analysed here: Poisson, Soneira–Peebles and Voronoi models described in Section 3. The side length is $300 h^{-1}$ Mpc.

plot, which could lead to wrongly interpret as fractals sets which clearly are not, as we show in Section 5.3 (see also Stoyan 1994, McCauley 1997).

3 THE K FUNCTION ON STOCHASTIC POINT PROCESSES

In order to test the usefulness of the statistic K and the accuracy of its estimator [equation (9)] we have calculated K and D_2 for three different point samples. They are controllable point processes for which we have some *a priori* knowledge of the expected behaviour of the K function. In order to compute as well the deviations from this theoretical behaviour when the empirical value is obtained on a point sample, we have analysed several realizations of each process, simulated in a cube of side $300 h^{-1}$ Mpc. Let us briefly describe the models analysed here.

i) Poisson sample. We generate 10 of these samples containing 1000 points each in order to test if our quantities behave in the expected way in the absence of any pattern.

ii) Soneira–Peebles model (S-P). Starting from a sphere of radius R and following Soneira & Peebles (1978), we randomly place η spheres of radius R/λ . In each of the resulting smaller spheres we do the same with spheres of radius R/λ^2 . We repeat this L times and consider the centres of the η^L spheres in the last level as our study objects. Although Soneira & Peebles (1978) add up N_r realizations of this kind, we simply generate one, which is known to be a single fractal (Martínez et al. 1990). The model is included inside a cube of side $300 h^{-1}$ Mpc. The values of the parameters we have chosen are $\eta = 2$, $\lambda = 2$, $L = 10$, and we have not allowed spheres in the same level to overlap. The expected value of D_2 can be analytically calculated for this model through the relation $D_2 = (\log \eta)/(\log \lambda)$ and, for this choice of the parameters, it turns out to be $D_2 = 1$. We have generated 10 of such samples.

iii) Voronoi sample. Essentially it is built (van de Weygaert 1991) by choosing points at random as centres of the cells of a Voronoi tessellation, which is produced by drawing planes equidistant to the nearest centres. Then a certain amount of objects (events of the point process) following a Gaussian distribution are put on and around the filaments which result of the intersection of two of those planes. We have analysed 5 realizations containing around 2500 points each.

All these point processes are shown in Fig. 2 and now we shall comment on the results of the K –function for the first three point processes, which are graphically represented in Fig. 3. For each sample, we plot the average of the function $K(r)$ calculated over the 10 realizations in the range of scales $[10, 100] h^{-1}$ Mpc, except for the Voronoi sample, which begins at $r = 1 h^{-1}$ Mpc. We plot the corresponding standard deviation as error bars. These are usually smaller than the size of the dot, probing thus the stability of the esti-

Figure 3. The functions $K(r)$ and $D_2(r)$ for the point processes i), ii) and iii). The straight continuous line corresponds to K_{Pois} .

mator. The dotted line represents the theoretical behaviour for a Poisson process. Let us mention that the depth up to which a statistic can be reliably calculated depends on the statistic itself and on the estimator used as well as on the geometry of the region. In our case, we have calculated $K(r)$ for $r \in [5, 150] h^{-1}$ Mpc and it follows the same trend as in the shorter interval $[10, 100] h^{-1}$ Mpc that we have plotted, except for more significant noise at very small scales. On the top of each panel we show the local dimension D_2 calculated as stated in Section 2. Note that we do not calculate D_2 basing ourselves on the K of each individual sample but on the average K of all the samples of a same process. Error bars are now 1σ uncertainties in the five-point weighted least squares fit.

In the estimation of the K function, we have checked that the lack of border correction (i.e., if we take $\omega_{ij} = 1 \forall i, j$) would underestimate significantly the amount of clustering, giving a false sense of regularity in the data.

Let us first point out that K has fully accomplished its mission as a detector of the scale of homogeneity. For the Poisson distribution we see that the estimator of $K(r)$ matches quite well the expected behaviour of equation (4). Moreover the value of the local dimension is nearly constant for the whole range of scales and $D_2 = 3$, with little fluctuations at small scales due to the small number of points.

The other two models clearly show clustering, since the function $K(r) \geq K_{\text{Pois}}(r)$. Note that homogeneity begins to be reached when the K curve of the sample falls on the theoretical straight line. The simple S-P clump is a pure fractal and hence it never reaches homogeneity; on the plot, this corresponds to the fact that the sample and theoretical lines do not coincide over the whole range of scales, being both straight lines with different slopes. The local dimension D_2 as a function of the scale r is practically a horizontal line at the theoretically predicted height, $D_2 \simeq 1$. This plateau is the fingerprint of fractal behaviour. The lacunarity of this fractal set, appreciated in Fig. 1, is responsible for the important error bars in the plot of D_2 . For larger values of r the estimates of K and hence of D_2 are biased by the edge correction, which assumes that the process is stationary and isotropic. Nevertheless for $r \leq 80 h^{-1}$ Mpc they give the correct result although the point process does not fulfill the required assumptions, showing that the method does not introduce spurious homogenization.

The different prescriptions used to generate the analysed point processes are reflected in the different shapes of K and in the behaviour of D_2 as a function of the scale. The Voronoi model used here is based on the population of the filaments; this can be seen in the fact that, for the smallest scales shown in the plot ($r < 8 h^{-1}$ Mpc), the dimension $D_2 \simeq 1$, corresponding to filamentary-like structures. At large scales we can appreciate a continuous variation of the local dimensionality from $D_2 \simeq 1$ to $D_2 \simeq 3$, corresponding to the scale at which homogeneity is reached ($r_{\text{hom}} \simeq 50 h^{-1}$ Mpc).

Figure 4. The different N -body simulations of the cluster distribution. The side of the box is $300 h^{-1}$ Mpc.

Figure 5. The standard correlation function $\xi(r)$ for the three cluster samples. We have plotted the average values over 10 realizations (only 8 for MDM) and the error bars correspond to 1σ deviations.

4 THE K FUNCTION ON SIMULATIONS OF THE CLUSTER DISTRIBUTION

We have furthermore analysed three sets of 10 N -body simulations of the distribution of clusters of galaxies (Croft & Efstathiou 1994a, 1994b). They have used a P^3M code to generate these samples, containing around 1000 clusters each of them in a cube of comoving side $300 h^{-1}$ Mpc.

i) Standard CDM. It has been generated from a CDM power spectrum that applies for models with low baryon density. The chosen values of the cosmological parameters are $\Omega = 1$ and $h = 0.5$.

iii) Mixed dark matter (MDM). It contains a massive neutrino component and CDM in a proportion so that $\Omega_{\text{total}} = 1$ and $\Omega_\nu = 0.3$, taking $h = 0.5$.

iii) CDM with cosmological constant (Λ -CDM). The values of the parameters are $\Omega = 0.2$, $h = 1$ and $\Lambda/(3H_0^2) = 0.8$.

All these simulations are shown in Fig. 4.

In Fig. 5 we have included, for the sake of comparison, the mean and 1σ errors of $\xi(r)$ for all the realizations of each N -body simulation. The estimator used is that of Rivolo (1986)

$$1 + \xi(r) = \sum_{i=1}^N \frac{N_i(r)}{nV_i}, \quad (10)$$

with $N_i(r)$ being the number of neighbours of the i th point in a shell centred at that point and having radii $r - dr/2$ and $r + dr/2$, and V_i being the volume of the intersection of that shell with the region D . There exists an analytical expression for V_i when D is a cube (Baddeley et al. 1993). The estimator in equation (10) gives smaller errors than the usual Davis & Peebles (1983) estimator. This question is being addressed at length in Pons-Bordería et al. (1998). In any case, the errors at large distances ($r > 10 h^{-1}$ Mpc) are very important. It is precisely in that region where it is especially interesting to use K , since ξ is dominated by the noise there and, on the contrary, errors on K are acceptable up to at least $1/3$ of the box sidelength. Although K is not as informative as ξ , in the same way that a distribution function is less informative than a density, it is better to have some information than to have none.

In Fig. 6 we present the results of the K function and the local dimension D_2 for the cluster simulations. It is quite evident that no clear plateau D_2 is observed, although two different regimes in its behaviour are appreciated. At small scales, ($r \leq 30 - 40 h^{-1}$ Mpc), D_2 increases with the scale

Figure 6. The same as Fig. 3 for the three simulations of the cluster distribution

Figure 7. The average and standard deviations of the K function for 8 subcubes of side $150 h^{-1}$ Mpc extracted from one of the MDM realizations. The dotted line corresponds to the whole simulation.

very slowly, with some cases showing behaviour compatible with a constant value of D_2 within the uncertainties. Nevertheless, the systematic increasing trend is observed for the three cases. In the second regime, for $r \geq 40 h^{-1}$ Mpc, the tendency to attain homogeneity is more clearly appreciated and D_2 increases more rapidly with the scale. This might be a good probe in order to test a possible fractal character of the geometry of the Universe.

It is interesting to observe how the MDM model and Λ -CDM have a similar effect with respect to the standard CDM, namely the increase of the amount of clustering at all scales and the delay of the achievement of homogeneity ($D_2 \simeq 3$). The scale at which this happens is $70 h^{-1}$ Mpc for MDM and Λ -CDM instead of $50 h^{-1}$ Mpc for CDM. Note that the stronger the clustering is, the larger the values of the K function. We see that, among the three N -body simulations, the strongest clustering is observed in MDM, followed by the Λ -CDM model and finally by the standard CDM. Regarding the dimension D_2 , standard CDM and Λ -CDM show similar values at small scales, while at large scales the agreement is between the MDM and the Λ -CDM models. K is none the less not able to distinguish between MDM and Λ -CDM.

In order to test the stability of this statistic when applied to smaller regions, we have subdivided one of the cubes (of $300 h^{-1}$ Mpc sidelength) containing a MDM simulation in 8 smaller cubes of $150 h^{-1}$ Mpc sidelength. We have calculated the K function for each of the subcubes up to $50 h^{-1}$ Mpc and, as we can see in Fig. 7, the statistic and its estimator are quite stable, since the results for the whole sample lie within the 1σ deviation from the average of K calculated on the smaller cubes. This is an illustration of the robustness of the estimator.

5 THE K FUNCTION ON GALAXY REDSHIFT SURVEYS

5.1 The surveys

In order to check if the K function produces reliable results when used on real data sets, we have applied it to four different galaxy catalogues. In all cases we have extracted volume-limited samples which are shown in Fig. 8; redshifts had been corrected from the heliocentric velocity with respect to the microwave background. Let us briefly describe the analysed samples:

5.1.1 CfA-I

The CfA-I catalogue with magnitude limit $m_B = 14.5$, compiled by Huchra et al. (1983) was based on Zwicky's angular catalog. We have extracted a complete volume-limited sample, which we shall call CfA80, lying inside the region delimited by galactic latitude $b > 40^\circ$, declination $\delta > 0$, distance to the Earth greater than $17h^{-1}$ Mpc and less than $80h^{-1}$ Mpc. It contains 185 galaxies, being the Coma cluster the most prominent feature in the sample. The volume comprised by it is $\simeq 3.13 \times 10^5 (h^{-1} \text{ Mpc})^3$ and subtends a solid angle of $\omega = 1.832605 \text{ sr}$.

5.1.2 Perseus–Pisces Supercluster (PPS)

The Perseus–Pisces catalogue has been compiled by Giovanelli & Haynes (1991), taking as a basis the old Zwicky catalogue. Its magnitude limit is $m_Z = 15.7$ and it covers (in equatorial coordinates) the region $\alpha \in [22^\circ, 24^\circ] \cup [0^\circ, 4^\circ]$, $\delta \in [0^\circ, 50^\circ]$. The most important feature contained in it is the Perseus–Pisces filamentary supercluster. The catalogue magnitudes have been corrected from interstellar absorption.

The extraction from this catalogue of a volume-limited sample has been performed by several authors, (see Ghigna et al. (1994) and references therein). We use the volume-limited sample extracted by Kerscher et al. (1997). They have neglected the zone most affected by galactic obscuration and restricted the sample to the area $\alpha \in [22^\circ.5, 24^\circ] \cup [0^\circ, 3^\circ]$, $\delta \in [0^\circ, 40^\circ]$. The depth is $79h^{-1}$ Mpc, it contains 817 galaxies and covers a solid angle of 0.76 sr, being the volume $\simeq 1.24 \times 10^5 (h^{-1} \text{ Mpc})^3$.

5.1.3 Stromlo–APM

The Stromlo–APM redshift survey was compiled by Loveday et al. (1996), based on the APM Bright Galaxy Catalogue (Loveday 1996). It consists of 1797 galaxies with a magnitude limit of $b_J \leq 17.15$ selected randomly at a rate of 1 in 20. The survey covers 4300 square degrees of the southern galactic sky, approximately defined in equatorial coordinates by $\alpha \in [21^\circ, 24^\circ] \cup [0^\circ, 5^\circ]$, $\delta \in [-72.5^\circ, -17.5^\circ]$. The survey redshifts have been transformed to the Local Group reference frame and K -corrections have been applied for different morphological types in the b_J system.

We have extracted a sample volume-limited to $200h^{-1}$ Mpc (assuming $q_0 = 0.5$), consisting of 387 galaxies. Distances are calculated according to the Mattig formula which for this choice reads as:

$$r = \frac{2c}{H_0} \left(1 - \frac{1}{\sqrt{1+z}} \right). \quad (11)$$

The fact that the sample is not complete is not a problem for the calculation of K since the function K is invariant under thinning (van Lieshout & Baddeley 1996).

5.1.4 IRAS 1.2 Jy

The *IRAS* 1.2 Jy survey was compiled by Fisher et al. (1995) based on the *IRAS* Point Source Catalogue (PSC) by Beichman et al. (1985). It contains 5321 galaxies and is complete to a flux limit of 1.2 Jy at $60\mu\text{m}$. The survey covers 87.6% of

Figure 8. Equal-area projections of some of the volume-limited samples analysed here: a) PPS (the north celestial pole is at the centre of the plot); b) The volume-limited sample of the Stromlo–APM redshift survey (now the south galactic pole is at the centre of the plot); c) Aitoff projection of the volume-limited sample of the *IRAS* 1.2 Jy survey (in galactic coordinates).

Figure 9. The K function for the CfA80 sample, the PPS sample and the Stromlo–APM survey. On top we show the local dimension D_2 (only where the correlation coefficient was at least 0.97) as a function of the scale r .

the sky, excluding only the Galactic plane region $|b| < 5^\circ$, a small region of sky not surveyed by *IRAS* and confused regions in the PSC.

We have extracted a sample volume-limited to $120h^{-1}$ Mpc from the survey. It contains 561 galaxies, comprising 270 galaxies in the northern galactic hemisphere and 291 galaxies in the southern hemisphere.

5.2 Results

We have typically analysed the K function up to 1/2 of the cubic root of the volume of each sample. The weighing term ω_{ij} in the denominator of the estimator \hat{K}_R in equation (9), which depends upon the geometry, is now measured by Monte Carlo integration since the shapes of the galaxy samples are not simple cubes but something much more complicated.

5.2.1 Optical samples

In Fig. 9 a plot of the results for the optically selected samples can be seen. On the top panel the results for the correlation dimension D_2 are shown, calculated where the function K fits reasonably well a power-law.

In the CfA80 sample, due to its shallowness, we have calculated K only up to $\simeq 30h^{-1}$ Mpc but it is enough to witness its transition to homogeneity. It is also remarkable the rapid change of its D_2 , which increases from 1.3 to almost 2.5 in less than $10h^{-1}$ Mpc.

The Perseus–Pisces survey presents clustering at all the scales we could analyse but it tends to homogeneity with increasing r , since its K value tends to K_{Pois} . The PPS sample is contained in too a small region to allow us inspection of K at very large scales. We have calculated the K function just up to $25 h^{-1}$ Mpc. Although it could be possible to fit a single power-law to the behaviour of the K function over the whole range with reasonable accuracy (Guzzo et al. 1991; Bonometto et al. 1994; Pietronero, Montuori & Sylos–Labini 1996), we are able to detect a decrease in the amount of clustering through the use of the local dimension D_2 , which goes from 1.8 at scales around $1 h^{-1}$ Mpc to 2.3 at scales around $20 h^{-1}$ Mpc. In order to go beyond $20 h^{-1}$ Mpc we have to analyse the other deeper samples.

Figure 10. The K function for the volume-limited samples of the 1.2 Jy *IRAS* catalogue. We use different marks for the North and South Galactic hemispheres. The differences between both are significant at small scales.

At small scales the values of K for the Stromlo-APM sample are noisier due to the sparseness of the sample. In the range $[5-25] h^{-1}$ Mpc, however, where the estimates are more reliable, there is a reasonable agreement among the results for the three samples.

It is interesting to notice that there is a kind of continuity between the D_2 values for the three optical samples. One can form an increasing curve which begins at small scales sampled by CfA80 with a value $D_2 \simeq 1.3$, joins the value $D_2 \simeq 2.2$ of PPS at intermediate scales and finally approaches the homogeneity value $D_2 \simeq 3$ with APM (which is the deepest sample), ruling out the idea of an unbounded fractal universe. This result is in agreement with a recent paper by Scaramella et al. (1998) in which they found evidences for a $D_2 = 3$ dimensionality for the ESO Slice project redshift survey and the Abell (ACO) clusters, using, as we do, comoving cosmological distances and K -corrections. Similar conclusions are reached by Wu, Lahav & Rees (1998) from the analysis of the X-ray Background and the Cosmic Microwave Background.

The increasing value of D_2 with the scale is less evident, although appreciable, for the PPS sample, in which the behaviour is a smooth increasing trend with oscillations that might be misinterpreted as a constant. In any case, it is interesting to remark that this survey has been selected to isolate one strong feature in the local Universe (Iovino et al. 1993), the Perseus-Pisces supercluster, a very big sheet-like structure, which contributes strongly to values close to 2 for the correlation dimension. However, as we have seen with the other analysed samples, this behaviour is particular of this sample due to a selection effect, and cannot be extrapolated to the whole Universe.

5.2.2 *IRAS* 1.2 Jy

Here we have analysed separately both galactic hemispheres by means of the K function. In Fig. 10 we see significant differences between the K function of the North and the South samples up to $20 h^{-1}$. The clustering seems stronger in the Southern hemisphere than in the Northern one. This result corroborates the findings of Kerscher et al. (1997). These authors found differences in the strength of the clustering between both hemispheres by means of the Minkowski functional and nearest-neighbour distributions. Also at small scales the values of K are typically larger for the *IRAS* 1.2 Jy sample than for the optical samples analysed previously. This result is in full agreement with the estimates of the correlation function at small scales reported in Fisher et al. (1994), Bonometto et al. (1994) and Loveday et al. (1995). However, at larger scales the K functions of both hemispheres approach in the same way the curve corresponding to a uniform Poissonian distribution.

5.3 Reliability of the results

One way of measuring the errors on the estimates of a statistical function such as $K(r)$ is based on the dispersion of its measures when applied to ensembles of artificial catalogues having similar statistical properties (Fisher et al. 1993; Hamilton 1993). The segment Cox processes (Stoyan, Kendall & Mecke 1995) are quite useful in this context. The particular model of Cox process (see also Pons-Bordería et al. 1998) used here has been generated in the following way: we scatter randomly in the space segments of length l , with λ_s being the mean number of segments per unit volume and, on those segments, we randomly distribute points so that a chosen λ_l be the mean number of points per unit length of the segments. The intensity of this process will be $\lambda = \lambda_l \lambda_s l$ and, as proven in Stoyan, Kendall & Mecke (1995), its K function will be given by:

$$K(r) = \begin{cases} \frac{4\pi}{3} r^3 + \frac{r}{\lambda_s l} (2 - \frac{r}{l}) & \text{if } r \leq l \\ \frac{4\pi}{3} r^3 + \frac{r}{\lambda_s} & \text{if } r > l \end{cases} \quad (12)$$

and one will be able to calculate D_2 analytically simply as:

$$D_2(r) = \frac{r}{K(r)} \times \frac{dK(r)}{dr}. \quad (13)$$

We have generated 10 such Cox processes containing between 1400 and 1600 points each inside a cube of side $100 h^{-1}$ Mpc. The values we have taken for the parameters are $l = 20$, $\lambda_s = 4 \times 10^{-5}$, $\lambda_l = 1.88$, $\lambda \simeq 1500/100^3$.

In Fig. 11 we can see the average empirical values of the estimates of $K(r)$ obtained by means of equation (9) together with the standard deviations. The expected theoretical function given by equation (12) is depicted as a solid line. As we can see, an empirical estimate of K calculated on 10 Cox processes reproduces quite satisfactorily the expected theoretical behaviour. Note that the variance of the number of counts in a bounded set for a Cox process is always bigger than in a Poisson process having the same intensity (Stoyan, Kendall & Mecke 1995). It is important to notice that the border correction has not destroyed the goodness of the estimator; in particular, it has not introduced spurious homogenization. Our estimator has worked successfully not only in the “easy” case of absence of structure which represent Poisson processes but it has also been able to reproduce quite exactly the very precise value of K for a clustered Cox process. This test gave us enough confidence to believe that the K results obtained from the galaxy samples effectively reflect the structure existing there.

The Cox processes used here also play an interesting role. They are a good example with which to prevent the naive use of fractals in the analysis of point fields as it has been anticipated by Stoyan (1994). In the inset of Fig. 11, we can see the function $\xi(r)$ expected for this process. The function is the sum of two power-laws $\xi(r) = Ar^{-2} + Br^{-1}$ with $A = (2\pi\lambda_s l)^{-1}$ and $B = -(2\pi\lambda_s l^2)^{-1}$. At short distances the first power-law dominates and therefore the function $\xi(r)$ can be nicely fitted to a power-law $\xi(r) \propto r^{-\gamma}$ with $\gamma = 2$ and this could lead to interpret that the point set is a fractal when clearly it is not (Stoyan 1994; McCauley 1997). Because in this regime $\xi(r) \gg 1$, the same can be said for the function $1 + \xi(r)$. Looking at the top panel of Fig. 11, we can see the behaviour of the empirical local dimension D_2 calculated over the average of the 10 realizations

Figure 11. Bottom panel: the average and 1σ deviation error bars of the function $K(r)$ for 10 realizations of the Cox point processes (solid discs). The inset shows the two-point correlation function of this stochastic model. Top panel: the local correlation dimension D_2 with 1σ uncertainties calculated by means of a five-point weighted log-log least square fit on the average of K . In both panels the solid line shows the theoretical values, while the dotted line in the bottom panel corresponds to $K_{\text{Pois}}(r)$.

of the Cox processes together with the 1σ deviations. The solid line represents the expected theoretical values [equation (13)]. Again we can see the reliability of the estimates. But what it is more interesting in this example is the long plateau observed in the plot of the correlation dimension. The value $D_2 \simeq 3 - \gamma \simeq 1$ remains nearly constant for a broad range of scales, due to the particular behaviour of the K function for this model. After the “fractal” behaviour, a transition to homogeneity is clearly appreciated in both D_2 and $K(r)$. It is interesting to remark the qualitatively similar behaviour between this figure and Fig. 9 in which we showed the same function for the analysed optical redshift surveys: a regime at small scales where the clustering is strong (with $K \gg K_{\text{Pois}}$) and where K can be fitted to a power-law. At larger scales, however the increasing behaviour of the local dimension D_2 with the scale and the continuous approximation of the function K to K_{Pois} are absolutely clear. At this point we want to remark that, in the same way that the term fractal is not appropriate for the Cox process, even having a correlation function decaying as a power-law at short scales (Stoyan 1994), the galaxy distribution, even holding a similar property, is not a fractal in a rigorous sense (McCauley 1997). However in a more loose use of the term fractal (Avnir et al. 1998), it could be appropriate to talk about a “fractal” regime to describe the range of scales where $K(r)$ follows a power-law, bearing in mind that a real self-similar point pattern, for example the Soneira-Peebles model described in section 3, verifies other conditions (self-similarity) apart from a power-law decaying correlation function.

6 CONCLUSIONS

We should like also to comment briefly on the relation of K with the correlation function $\xi(r)$. Both play their role in the analysis of the point pattern and, as Stoyan & Stoyan (1996) say, their relation is similar to that between the distribution function and the probability density function in classical statistics. The use of a cumulative quantity such as K avoids binning in distance, which is often a source of arbitrariness for ξ (Ripley 1992). Let us explain why ξ does suffer from the hindrance of splitting the information into disjoint bins. When one estimates $\xi(r)$ in $[r, r+dr]$, it is assumed that within that bin the correlation function is constant, and since this is obviously not true, the larger the bin the larger the error, but we cannot make arbitrarily small the size dr of the bin, because in that case we would not find any pairs. In other words, $\xi(r)$ has an additional source of bias, not present in K , due to the smoothing caused by av-

eraging over pairs of points close to but not exactly r units apart of each other (Stein 1996).

The correlation length ($r_0|\xi(r_0) = 1$) is just the scale at which the density of galaxies is, on average, twice the mean number density. At smaller scales the pair correlations are due to non-linear perturbations, but homogeneity is not reached till $\xi(r_{\text{hom}}) \sim 0$. The main interest of K is that it permits us to study clustering precisely in that “difficult” range where $r_0 < r < r_{\text{hom}}$, which cannot be reached by ξ because in this range the errors on the estimates of ξ are comparable with their values, while the difference $K - K_{\text{Pois}}$ is still meaningful.

As a concluding remark, we want to stress that an unbiased estimator of a quantity related with the correlation integral, known as the K function, has been applied to cosmological simulations and galaxy samples. This function, extensively used in the field of spatial statistics, provides a nice measure of clustering. The border correction used here does not waste any data points and does not introduce spurious homogenization, giving reliability to the evaluation of this function at large scales. Through the slope of K we are able to calculate D_2 , which is an indicator of a possible fractal behaviour of the point process at a given scale range. The clear physical meaning of K and D_2 helps us easily interpret the clustering properties of different models of structure formation at different scales.

Regarding the analysis of the galaxy redshift surveys, we have seen that the estimator of the K function is robust in the sense that it does not depend on the shape of the study region and provides us with reliable information about the point patterns over a wide range of scales. The behaviour of the local dimension D_2 for the real galaxy samples is particularly interesting to proponents of various fractal models of large-scale structure. If a constancy of D_2 with the scale is a necessary condition for having a fractal point pattern (although it should not be sufficient as we have seen with the Cox process [see also Stoyan (1994) for more examples]), it is a neat conclusion of our analysis that the galaxy distribution does not even hold the necessary condition. The analysis presented here will provide a conclusive test to discover the scale at which the distribution of the matter in the Universe is really homogeneous when applied, in the near future, to the bigger and deeper galaxy catalogues which will be soon ready for common use.

ACKNOWLEDGEMENTS

This work has been partially supported by an EC Human Capital and Mobility network (contract ERB CHRX-CT93-0129) and by the Spanish DGES project n. PB96-0707. We thank prof. Stoyan for bringing the Cox model to our attention and for useful conversations and comments. We thank R. Croft, S. Paredes, R. Trasarti-Battistoni and R. van de Weygaert for kindly allowing us to use their samples and programs, as well as T. Buchert, J. Schmalzing, M. Stein and specially M. Kerscher for very interesting discussions and comments. The authors want to thank the anonymous referee for his/her valuable comments and suggestions.

REFERENCES

Avnir, D., Biham, O., Lidar, D., & Malcai, O. 1998, *Science* 279, 39

Baddeley, A.J., Moyeed, R.A., Howard, C.V., & Boyde, A. 1993, *Appl. Statist.* 42, 641

Bartlett, M.S. 1964, *Biometrika* 51, 299

Beichman, C.A., Neugebauer, G., Habing, H.J., Clegg, P.E., & Chester, T.J., 1985, IRAS Catalogs and Atlases, Washington Bonometto, S., Iovino, A., Guzzo, L., Giovanelli, R. & Haynes, M., 1994, *ApJ* 419, 451

Borgani, S., Martínez, V.J., Pérez, M.A., & Valdarnini, R. 1994, *ApJ* 435, 37

Buchert, T., & Martínez, V.J. 1993, *ApJ* 411, 485

Cappi, A., Benoist, C., da Costa, L.N., & Maurogordato, S. 1998, *astro-ph/9804085*, *A&A* (in press)

Coleman, P.H., & Pietronero, L. 1992, *Phys. Rep.*, 213, 31

Croft, R.A.C., & Efstathiou, G. 1994a, *MNRAS* 267, 390

Croft, R.A.C., & Efstathiou, G. 1994b, *MNRAS* 268, L23

Davis, M., & Peebles, P.J.E. 1983, *ApJ* 267, 465

Diggle, P.J., 1983, *Statistical Analysis of Spatial Point Patterns*. Academic Press, London

Doguwa, S.I. & Upton, G.J.G.. 1989, *Biom. J.* 5, 563

Domínguez-Tenreiro, R., Gómez-Flechoso, M.A. & Martínez, V.J. 1994, *ApJ* 424, 42

Dubuc, B., Quiniou, J.F., Roques-Carmes, C., Tricot, C. & Zucker, S.W. 1989, *Phys. Rev A*, 39, 1500

Einasto, J., & Gramann, M. 1993, *ApJ* 407, 443

Fisher K.B., Davis M., Strauss M.A., Yahil A., Huchra J.P., 1993, *ApJ*, 402, 42

Fisher K.B., Davis M., Strauss M.A., Yahil A., Huchra J.P., 1994, *MNRAS*, 266, 50

Fisher, K.B., Huchra, J.P., Strauss, M.A., Davis, M., Yahil, A., & Schlegel, D. 1995, *ApJS* 100, 69

Geller, M.J., & Huchra, J.P. 1989, *Science*, 246, 897

Giovanelli, R., & Haynes, M. 1991, *ARA&A*, 29, 499

Ghigna, S., Borgani, S., Bonometto, S.A., et al. 1994, *ApJ Let.*, 437, L71

Guzzo, L., Iovino, A., Chincarini, G., Giovanelli, R. & Haynes, M.P. 1991, *ApJ*, 382, L5

Guzzo, L. 1997, *New Astronomy* 2, 517

Hamilton, A.J.S. 1993, *ApJ*, 417, 19

Huchra, J.P., Davis, M., Latham, D., & Tonry, J. 1983, *ApJ Suppl.*, 52, 89

Iovino, A., Giovanelli, R., Haynes, M.P., Chincharini, G. & Guzzo, L. 1993, *MNRAS*, 265, 21

Kerscher, M., Pons-Bordería, M.J., Schmalzing, J., Trasarti-Battistoni, R., Buchert, T., & Martínez, V.J. 1997, *astro-ph/9712098*

Kerscher, M., Schmalzing, J., Buchert, T., & Wagner, H. 1998, *A&A* 333, 1

Kirshner, R.P., Oemler, A. Jr., Schechter, P.L., & Shectman, S.A. 1981, *ApJ* 248, L57

Loveday, J., Maddox, S.J., Efstathiou, G., & Peterson, B.A. 1995, *ApJ* 442, 457

Loveday, J., Peterson, B.A., Maddox, S.J., & Efstathiou, G. 1996, *ApJ Suppl* 107

Loveday, J. 1996, *MNRAS* 278, 1025

Martínez, V.J., Jones, B.J.T., Domínguez-Tenreiro, R., & van de Weygaert, R. 1990, *ApJ* 357, 50

Martínez, V.J., & Coles, P. 1994, *ApJ* 437, 550

Martínez, V.J., Paredes, S., Borgani, S., & Coles, P. 1995, *Science* 269, 1245

McCauley, J.L. 1997, *astro-ph/9703046*

Neymann, J., & Scott, E. 1952, *ApJ* 116, 144

Neymann, J., & Scott, E. 1955, *AJ* 60, 33

Park, C., Vogeley, M.S., Geller, M.J., & Huchra, J.P. 1994, *ApJ* 431, 569

Peebles P.J.E. 1980, *The Large Scale Structure of the Universe*. Princeton University Press, Princeton

Peebles, P.J.E. 1989, *Physica D*, 38, 273

Peebles, P.J.E. 1993, *Physical Cosmology*. Princeton University Press, Princeton

Pietronero, L., Montuori, M., & Sylos Labini, F., 1996, in Turok N., ed., *Critical Dialogues in Cosmology*. to appear, *astro-ph/9611197*

Pons-Bordería, M.J., Martínez, V.J., Stoyan, D., Stoyan, H., & Saar, E., 1997, submitted

Rivolo, A.R. 1986, *ApJ*, 301, 70

Ripley, B.D. 1976, *J. Appl. Prob.*, 13, 255

Ripley, B.D. 1977, *J. Royal Statist. Soc.*, 39, 172

Ripley, B.D., 1981, *Spatial Statistics*. John Wiley & Sons, NY

Ripley, B.D. 1992, in Feigelson, E.D. & Babu, G.J., ed., *Statistical Challenges in Modern Astronomy*. Springer-Verlag, NY, p. 102

Scaramella, R., et al. 1998, *A&A*, in press (*astro-ph/9803022*)

Smoot, G.F., et al. 1992, *ApJ*, 396, L1

Soneira R.M., & Peebles P.J.E. 1978, *AJ* 83, 845

Stein, M. 1996, in Feigelson, E.D. & Babu, G.J., ed., *Statistical Challenges in Modern Astronomy II*. Springer-Verlag, NY

Stoyan, D., Kendall, W.S., & Mecke, J. 1995, *Statistic Geometry and its Applications*. Springer-Verlag, Berlin

Stoyan, D. 1994, *Statistics* 25, 267

Stoyan, D., & Stoyan, H., 1994, *Fractals, Random Shapes and Point Fields*. John Wiley & Sons, Chichester

Stoyan, D., & Stoyan, H. 1996, *Biom. J.* 38, 259

Stoyan, D., & Stoyan, H. 1998, preprint 98-3 Technische Universität Bergakademie Freiberg

Szapudi, I., & Szalay, A.S. *astro-ph/9704241*

Tadros, H., & Efstathiou, G. 1996, *MNRAS* 282, 1381

Upton, G.J.G., & Fingleton, B. 1987, *Spatial Data Analysis by Example*, Vol. 1. John Wiley & Sons, NY

van de Weygaert, R., 1991, Ph.D. Thesis, Rijksuniversiteit Leiden

van Lieshout, M.N.M., & Baddeley, A.J. 1996, *Statistica Neerlandica*, 50, 344

Wu, K.K.S., Lahav, O., & Rees, M.J. 1998, *astro-ph/9804062*, submitted to *Nature*

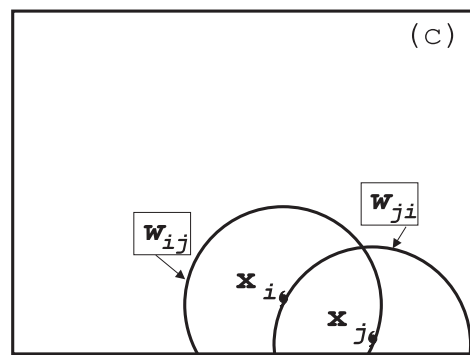
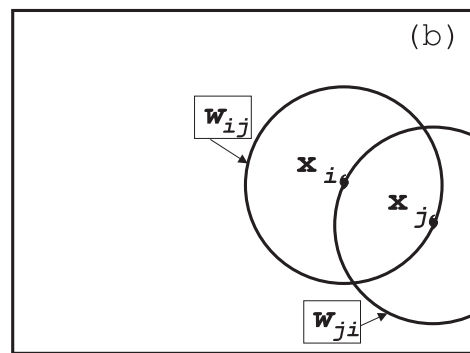
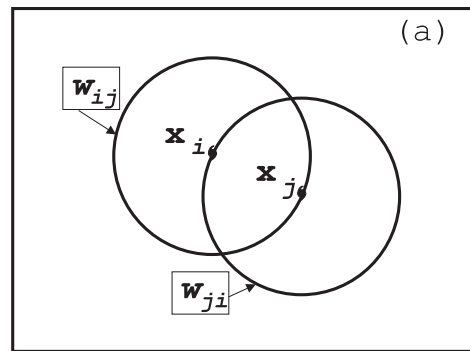


Figure 1

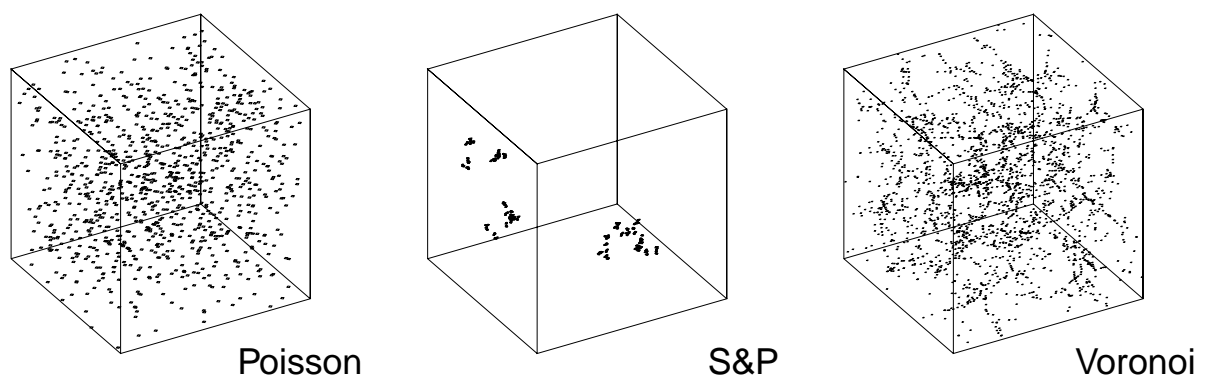


Figure 2

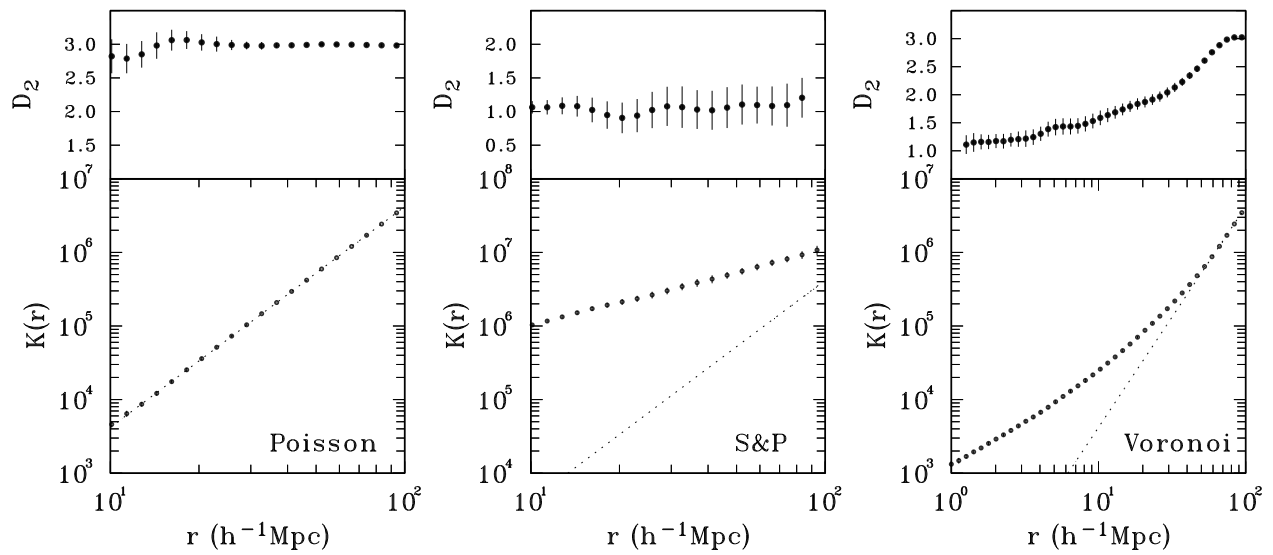


Figure 3

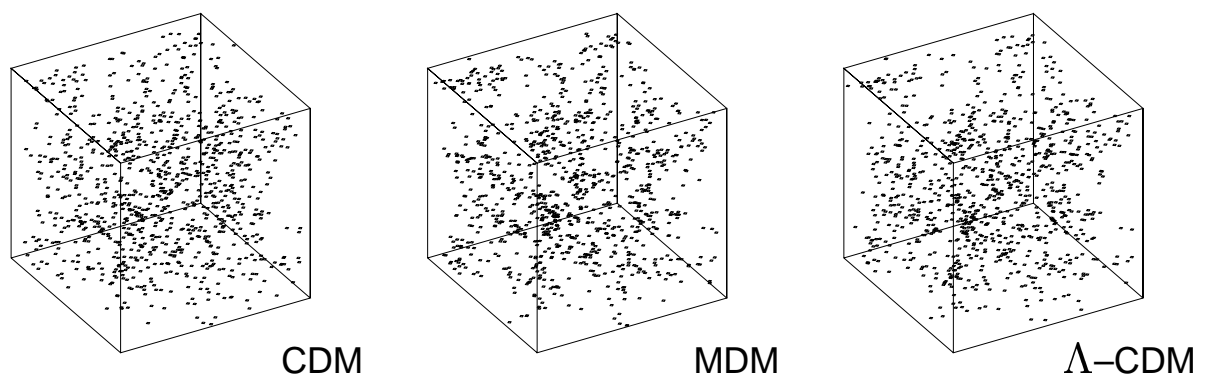


Figure 4

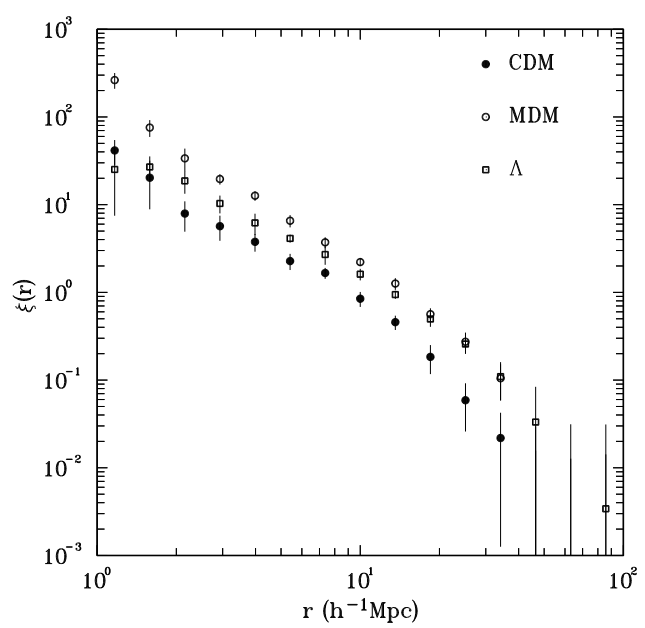


Figure 5

Figure 6

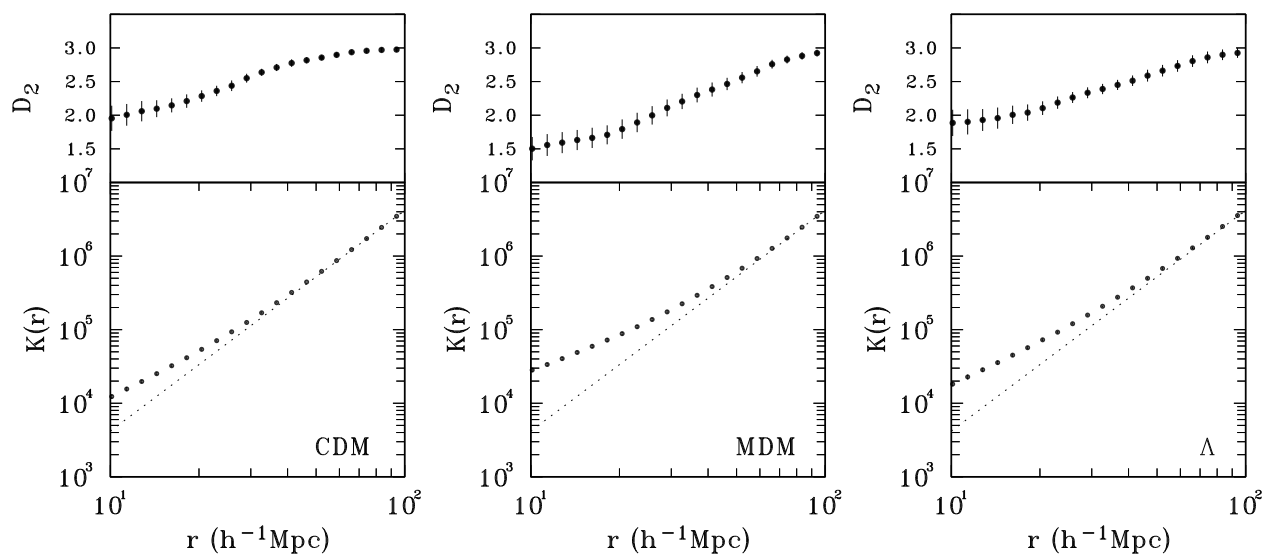
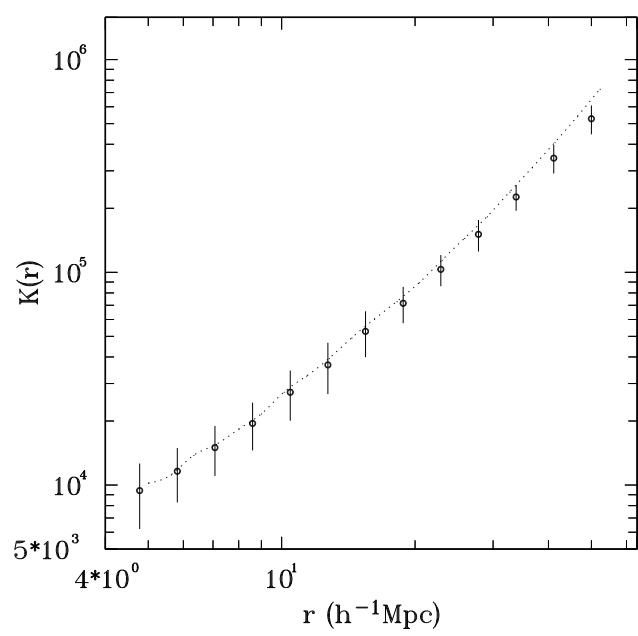


Figure 7



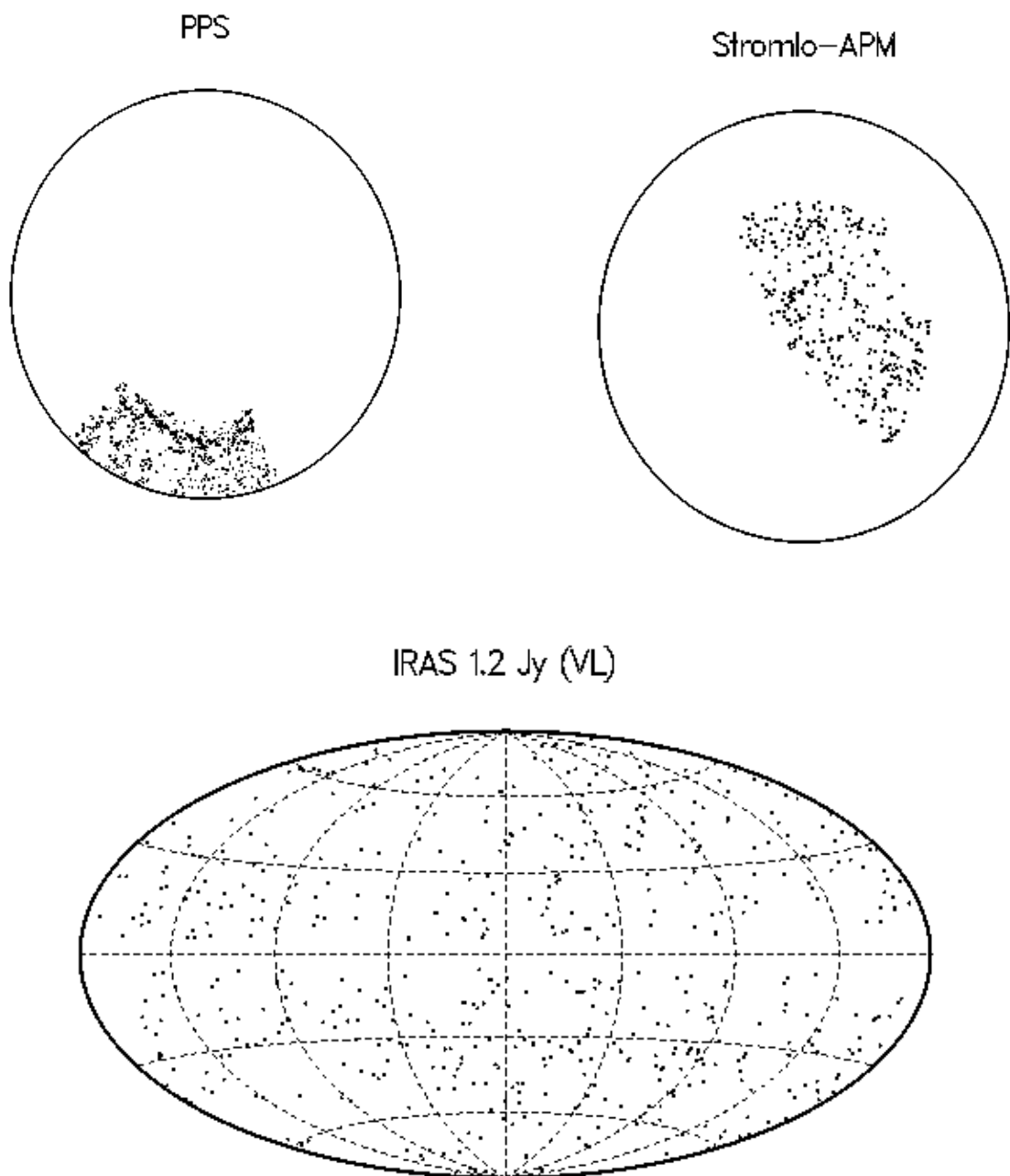


Figure 8

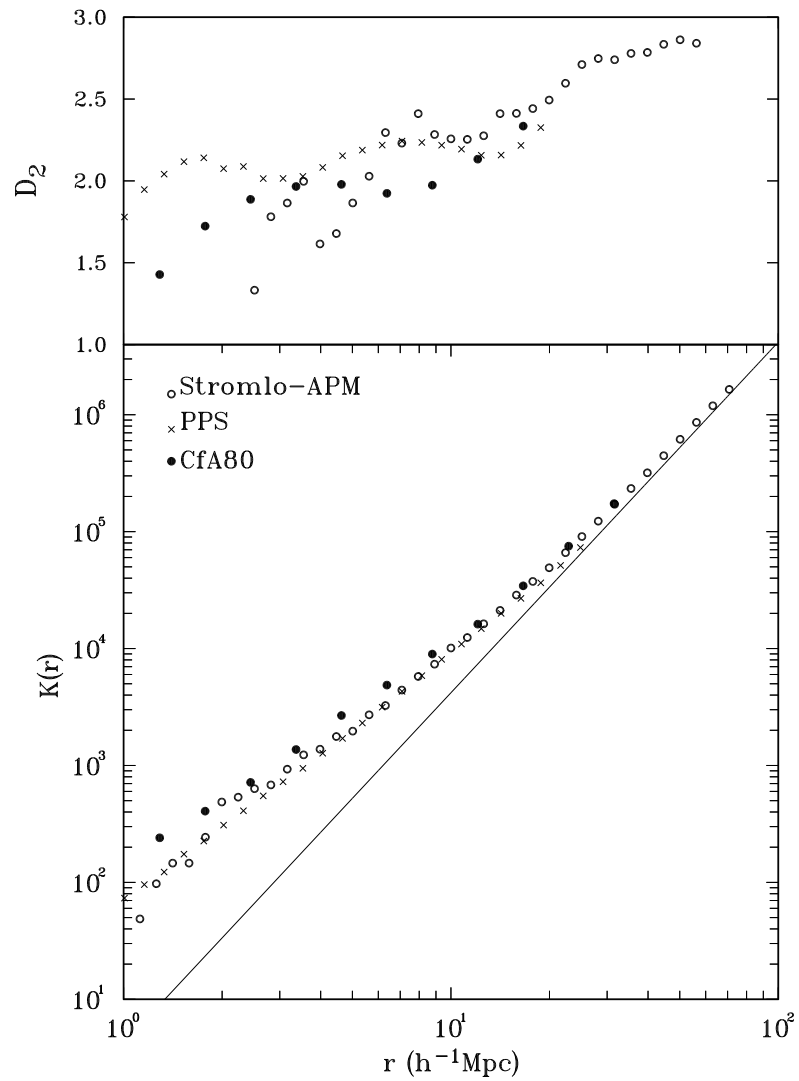
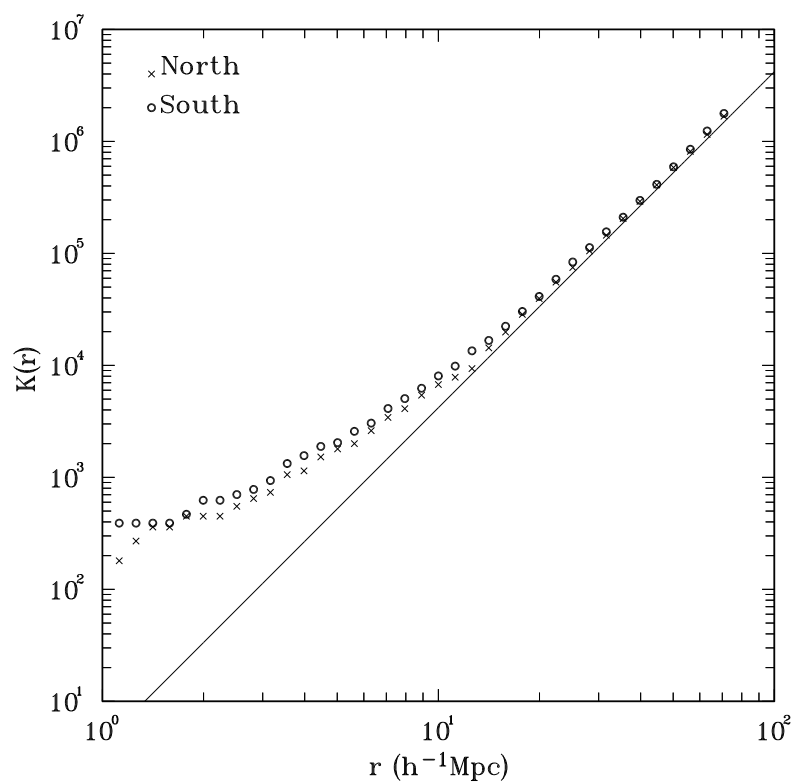


Figure 9

Figure 10



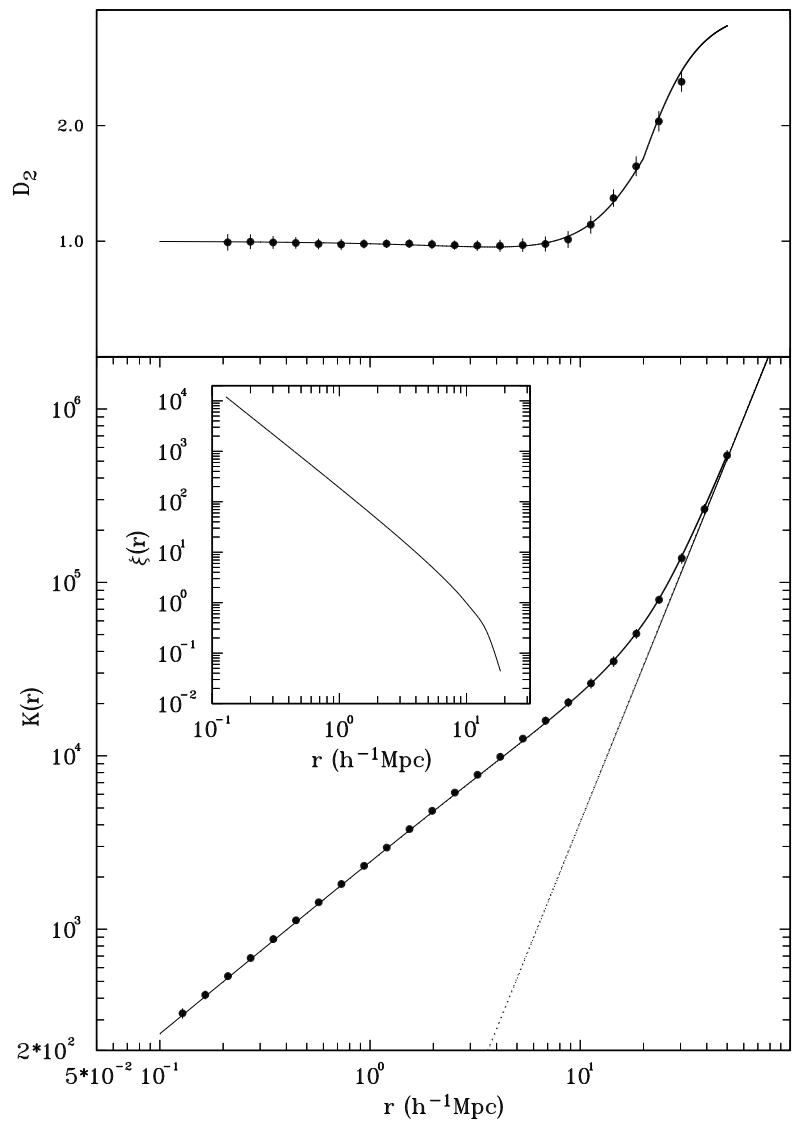


Figure 11